Effect of Shaft Rotation on the Incompressible Flow in a Labyrinth Seal

J. A. Demko*
General Dynamics, Fort Worth, Texas
and
G. L. Morrison† and D. L. Rhode‡
Texas A&M University, College Station, Texas

A computational/experimental study was conducted concerning the incompressible flow in a labyrinth seal at low leakage rates over a wide range of seal rotation rates. The predictions were obtained using a finite-difference code that utilized a higher order differencing scheme (QUICK) to reduce the effects of false diffusion. Measured inlet boundary conditions for the axial and swirl velocity components as well as turbulence kinetic energy were employed. This yielded fair agreement between velocity predictions and hot-film anemometer measurements. The effects of seal rotation rate on the overall pressure drop are presented in terms of a loss coefficient. It was determined that when the rotation rate is increased beyond a certain point, a second recirculation zone (SRZ) forms inside the seal cavity. This dramatically alters the flowfield in the cavity and results in a substantial increase in the pressure drop across it. A flow map is presented indicating the approximate rotation rate required to produce this phenomenon at a given leakage rate. Unfortunately, for most practical applications, the SRZ will not form until an extremely high shaft speed is reached.

Nomenclature

C_L	= dimensionless pressure loss coefficient
C_μ	= turbulence model constant
c	= seal clearance
D_ϕ	= diffusion coefficient of ϕ
k	= turbulence kinetic energy
L	= length of a labyrinth seal
$\dot{m}$	= mass flow rate through the labyrinth seal
P	= pressure
P_e, P_i	= static pressure at the cavity exit and inlet plenum, respectively
P_{ow}	= stator wall pressure at inlet to computational domain
P^*	= dimensionless pressure
Re	= axial Reynolds number
r_{sh}	= radius of the shaft
S_ϕ	= source term of ϕ in the generalized ϕ transport equation
Ta	= Taylor number
U_o	= spatially averaged inlet axial velocity
U^*, V^*, W^*	= dimensionless mean velocity in the axial, radial, and azimuthal directions
u, v, w	= time mean velocity components in the axial, radial, and azimuthal directions
W_{sh}	= peripheral velocity of the shaft
ε	= turbulence dissipation rate of kinetic energy
μ	= absolute viscosity
μ_{eff}	= effective turbulent viscosity
ν	= kinematic viscosity
ρ	= density
ϕ	= generalized variable quantity
ψ^*	= dimensionless stream function
Subscript	
sh	= evaluated at the shaft

I. Introduction

LABYRINTH seals are often used in locations where contact seals cannot be used due to large displacements of the rotating shaft, severe operating conditions, or sealing material limitations. Such conditions are frequently encountered in high-performance turbomachinery. Some examples are shaft sealing applications in pumps and between compressor or turbine stages in gas turbine engines. Another gas turbine application is to control the leakage flow between the turbine blade tips and the stator wall. Leakage control in these locations is known to affect the overall performance and the efficiency of these engines.[1]

The labyrinth seal considered in this study is composed of a series of identical generic cavities, as shown in Fig. 1. The shaft is concentric with respect to the stator housing. The teeth are located on the shaft so as to provide rectangular-shaped cavities, as indicated. The flow enters and exits a given cavity through the small annular clearance between a tooth and stator wall. The incompressible leakage flow is assumed to be turbulent, with at least one recirculation zone within each cavity.

Stoff[2] performed a combined computational/experimental investigation for a seal with a rectangular cavity geometry. Using pressure-velocity variables, a computer code with the k-ε model of turbulence was developed to obtain results that correlated well with his experimental measurements. Stoff presented results for swirl velocity only at one axial location, along with limited details about the various turbulence quantities, such as turbulence kinetic energy and dissipation rate. He did illustrate, through the use of velocity vector plots, the effects of swirl on the flow patterns for low leakage conditions.

Rhode et al.[3] also predicted labyrinth flowfields and considered both a generic rectangular labyrinth seal cavity geometry as well as a contoured shape. This work reduced numerical

Received April 23, 1987; revision received Sept. 10, 1988.

*Engineering Specialist. Member AIAA.
†Professor, Mechanical Engineering Department. Senior Member AIAA.
‡Associate Professor, Mechanical Engineering Department. Member AIAA.

diffusion by applying a higher order differencing scheme (QUICK) than that used by Stoff. Rhode et al.[3] also compared their predictions with some measured wall pressure distributions and found reasonable agreement.

A wide range of labyrinth seal configurations was evaluated in Refs. 4 and 5. After an extensive parametric study was conducted in each investigation using a finite-difference computer code, the optimized design was fabricated and tested. The measurements from these two studies showed leakage reductions over the existing impeller wear ring seal of 67 and 32%, respectively.

The current work consists of a combined experimental and computational investigation of the incompressible flow through labyrinth seals at low-leakage conditions. The predictions were made using measured values for inlet boundary conditions. In the past, labyrinth seal simulations relied on the assumption that the flow was streamwise periodic. Hence, the inlet values were obtained using corresponding outlet values from the previous iteration.

II. Computational Formulation

The assumed steady flow is modeled employing the fully elliptic, Reynolds-averaged, Navier-Stokes equations for turbulent flow. Specifically, these are comprised of momentum equations in the x, r, and θ directions, as well as the conservation of mass equation. Closure is provided via the use of the two-equation k-ε turbulence model, as outlined by Launder and Spalding.[6] All of these equations may conveniently be expressed in the common form for axisymmetric, steady flows:

$$\frac{1}{r}\left[\frac{\partial}{\partial x}(\rho u r\phi)+\frac{\partial}{\partial r}(\rho v r\phi)-\frac{\partial}{\partial x}\left(rD_\phi\frac{\partial\phi}{\partial x}\right)-\frac{\partial}{\partial r}\left(rD_\phi\frac{\partial\phi}{\partial r}\right)\right]=S_\phi \tag{1}$$

For example, the momentum equation in the x, r, or θ direction results when $\phi = u, v,$ or w, respectively. An auxiliary relation for the effective eddy viscosity, which is based on the Boussinesq eddy viscosity concept, is utilized. It is given by

$$\mu_{\text{eff}}=\frac{C_\mu\rho k^2}{\varepsilon}+\mu_l \tag{2}$$

The k-ε model is probably the most popular and widely used turbulence closure model.[7] This model has been applied to nonswirling, nonreacting flows as well as swirling and reacting flows. The k-ε model is considered to be a reasonable compromise between model sophistication and computational work. Researchers have sometimes obtained disappointing results when applying it to swirling flows. The basis for this is that the k-ε model was derived assuming an isotropic eddy viscosity. This assumption is not valid for some swirling flows. Recently, Abujelala and Lilley[8] have optimized the model constants for swirling flows, but they found little improvement in their computational results. The standard k-ε model was used since there is a wealth of experience with it; also, there is a lack of confidence that other alternatives would offer significant improvements.

The finite-difference form of each ϕ equation is obtained by integrating Eq. (1) over a finite-difference control volume via application of the Gauss divergence theorem. Thus, the convection and diffusion terms become surface integrals of convective and diffusive fluxes, whereas the source term is approximated by a linear function of ϕ. A typical computational domain is illustrated in Fig. 2, using a simplistic coarse grid.

Accurate representation of the convective fluxes is hindered by the false diffusion present when using upwind differencing.[9] False diffusion is a second-order truncation error that can become quite substantial under certain flow conditions. This inaccuracy may be substantially larger than the actual diffusion present, which may obscure important details. The QUICK differencing scheme[10] had previously been implemented into the convection terms of the computer code employed. The merits of this procedure over the standard Hybrid upwind/central differencing scheme have been attested to by several authors.[11-13] It was also shown by Rhode et al.[3] that there can be a substantial savings in computer time for a given level of accuracy using QUICK instead of the hybrid scheme through the use of a more coarse grid.

Measurements were employed as inlet boundary conditions to the fifth cavity as much as possible in order to enhance the predicted realism. However, there is uncertainty in these inlet measurements, especially for the low leakage cases. Also, various measurements at important locations near walls were not feasible with the present instrumentation. Hence, a least-squares polynominal curve fit of these inlet values was employed to estimate values for certain locations. Turbulence dissipation ε was specified at the inlet using a standard length scale assumption as

$$\varepsilon=\frac{C_\mu k^{3/2}}{0.03\,c} \tag{3}$$

Along solid surfaces, well-known wall functions are used to incorporate the boundary conditions for the momentum equations and the turbulence energy generation terms. A detailed discussion of the use of wall functions for flows near stationary boundaries, along with an appropriate specification for turbulence dissipation near a wall, were discussed by Launder and Spalding.[6,14]

The solution of the difference equations was obtained via the SIMPLER algorithm, as presented by Patankar.[15] Convergence was considered obtained when the summation of the residual source magnitudes over the flowfield was less than 0.4% of the inlet reference values.

Grid independence testing was conducted by comparing the solutions for one flow case on a 20 × 20 grid, a 34 × 34 grid, and a 43 × 42 grid. The results of this comparison indicated that the 20 × 20 grid was not grid independent and that the

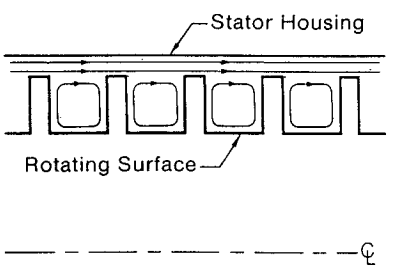

Fig. 1 Generic labyrinth seal configuration showing expected streamlines.

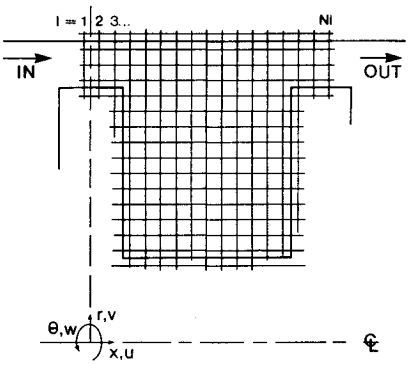

Fig. 2 Computational domain for a labyrinth seal cavity illustrating a coarse grid.

Table 1 Summary of flow conditions

U(m/s)	Re	Ta	Ta/Re	Formation of second vortex
1.15	17,880	0	0	N
1.09	16,920	7,600	0.45	I
1.11	17,340	19,000	1.10	S

S = second vortex formed. I = incipience of second vortex. N = no evidence of formation of second vortex.

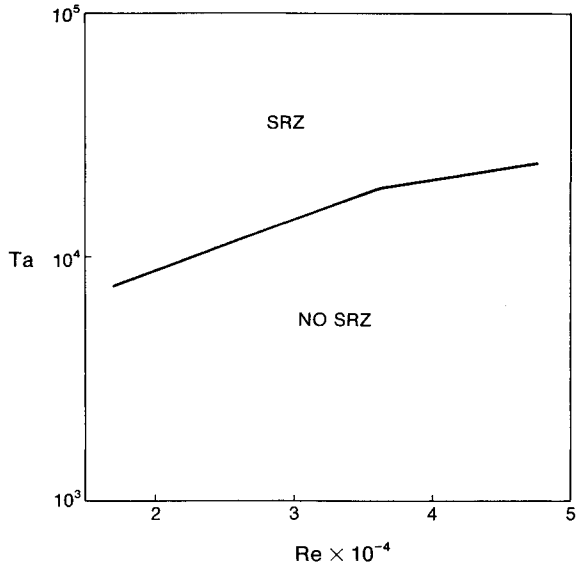

Fig. 3 Predicted flow map indicating the region where a second recirculation zone (SRZ) exists.

34 × 34 grid solution was essentially identical to the 43 × 42 grid solution.

III. Experimental Approach

The measurements used in this work were made with a TSI 1050 constant temperature anemometer, with a TSI 1247A-10 W crossed film sensor. The instantaneous voltage readings, as well as the required data reduction, were performed using a MINC PDP 11/23 microcomputer. The procedure utilized provided measured values for axial and swirl velocity components and turbulence kinetic energy estimates for several locations inside the flowfield. The measurement technique and data reduction method are both discussed by Demko.[16]

IV. Results

Table 1 lists the corresponding mean axial velocity component, axial Reynolds number, Taylor number, and the ratio of Taylor number to Reynolds number for all of the axial flow rates studied. These dimensionless numbers are defined by the following expressions:

$$Re = \frac{U_o(2c)}{\nu} \qquad Ta = \frac{W_{sh}c}{\nu}\sqrt{\frac{c}{r_{sh}}} \tag{4}$$

where W_{sh} is the velocity of the peripheral edge of a labyrinth seal tooth. The tooth thickness and clearance of the seal configuration investigated are both 0.635 cm. The axial spacing between the teeth is 1.635 cm and the tooth height is 1.905 cm. Further, there are a total of five identical cavities and the results pertain specifically to the last of these.

The relative importance of swirl to axial momentum can be gauged by the Ta/Re ratio. It was found that when swirl is large compared to the axial flow, a second vortex develops in the cavity. In the case of a labyrinth seal, this is a desirable

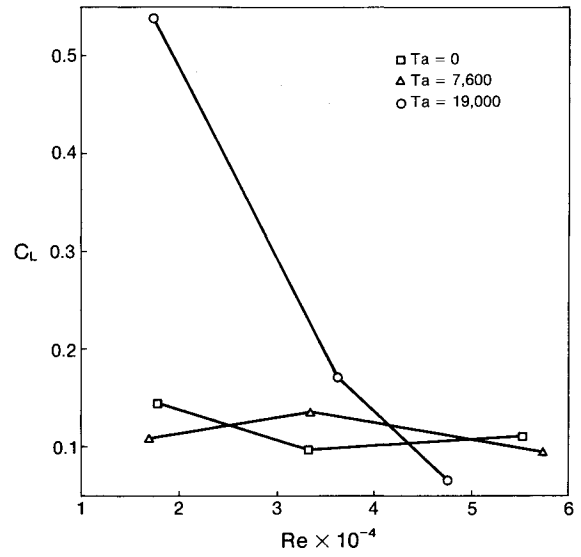

Fig. 4 Predicted energy loss coefficient.

phenomenon, since it significantly increases the pressure drop across a cavity for a given leakage rate. Also tabulated in Table 1 is the nature of the flowfield regarding the number of vortices predicted. A flow map indicating incipience of the second recirculation zone is given in Fig. 3 for a wide range of axial flowrates. From leakage test data presented in Ref. 17, it may be shown that a second recirculation zone will not form for conventional labyrinth seal applications, since the required shaft rotation rate would be prohibitively high. For example, consider a seal with a shaft diameter of 7.72 cm, and a clearance of 0.0178 cm. For a particular pressure drop, the axial Reynolds number was found to be 7000 for a corresponding Taylor number of 262 at 5000 rpm. For the second vortex to form at this leakage rate, the Taylor number would have to be greater than 5000 corresponding to an rpm over 100,000. Thus, the formation of the second vortex is unlikely to occur under normal operating conditions for such a see-through seal.

Based on the energy equation for duct flows, a leakage loss coefficient may be defined as follows:

$$C_L = \frac{2}{U_o^2}\left[\frac{P_i - P_e}{\rho} + g(z_i - z_e)\right] \tag{5}$$

The loss coefficient was obtained from the computed results. It is plotted as a function of Reynolds number in Fig. 4. At the highest Taylor number of 19,000, the low values of Re enable a second vortex to develop. This is the cause of the dramatic increase in the loss coefficient in this region. The following sections will provide a detailed examination of the incompressible flowfield in the labyrinth seal cavity at low leakage conditions.

At a Reynolds number of approximately 17,500, the three Taylor numbers considered give rise to flow patterns containing: 1) one large recirculation zone, 2) one large and one small zone, and 3) two large zones in the order of increasing Taylor number. For these cases, the ratios of Ta/Re are 0.0, 0.45, and 1.10. The first and last of these flow patterns are shown in the predicted streamline plots shown in Figs. 5a and 5b. Considering the streamlines for $Ta = 0$, there appears to be no significant differences from other reported flows without swirl.[2,3] Increasing the Taylor number to 7600 distorts the flowfield by producing a curved dividing streamline between the teeth. Also, a second recirculation zone (SRZ) begins to appear in the computations in the lower downstream corner. At the high Taylor number of 19,000, the two recirculation zones share a nearly equal portion of the flow space in the cavity. There also is a second stagnation point at $r/R = 0.93$

on the side of the downstream tooth. A limiting case was predicted by Stoff[2] where Ta/Re approaches infinity. This is achieved with no axial flow through the seal. He showed, for this case, that the two vortices are symmetrical about the center of the cavity. When an axial flow is imposed through the seal, the vortices become skewed, as shown in Fig. 5b.

The profiles of U^* velocity are shown in Fig. 6. For $Ta = 0$, the characteristics are similar to those previously reported.[2,3] At $Ta = 7600$, the initial effects of swirl begin to appear near the rotor wall. In higher leakage cases, these effects are present to a lesser degree. For the high swirl case with $Ta = 19{,}000$, the velocities have become positive next to the rotor. This is a result of the SRZ now covering a significant portion of the flow region.

At higher Taylor numbers, there are many interesting features to be found in the V^* profile shown in Figs. 7a and 7b. By comparing Taylor numbers of 0 and 7600 (not shown), several interesting differences appear. First, for $Ta = 7600$ at $r/R = 0.95$, there is a significant amount of V^* along most of the profile, except near $x/L = 0.5$. Secondly, the radial velocity along the upstream tooth increases in magnitude relative to the $Ta = 0$ case. This is due to centrifugal forces that result from the swirl velocity. The radial velocity distribution for $Ta = 19{,}000$, the highest value encountered in this study, is very much different from the previous cases. Notice that the radial velocities are all positive along the tooth walls. Sufficient centrifugal force is produced by the swirl along the tooth walls to direct the fluid radially outward in these regions. Any negative V^*, which must be present to satisfy continuity, must occur in the central region of the cavity.

Predictions of swirl velocity are in agreement with measurements for $Ta = 7600$ and 19,000, as shown in Fig. 8. At $Ta = 19{,}000$, the radial W^* profiles have slightly different shapes at $x/L = 0.318$, 0.5, and 0.682. The abrupt slope change, which occurs at about $r/R = 0.95$ for $Ta = 7600$, smooths out considerably, due to turbulent diffusion.

Radial pressure distributions for the highest and lowest Taylor numbers are presented in Fig. 9. For $Ta = 0$, the leakage flow pressure increases in the streamwise direction for the entire length of flow. Although some of the pressure energy is dissipated through turbulence mechanisms, this was not sufficient to overcome the pressure increase due to gravity head, as the flow was in the direction of the gravity force.

Increasing the Taylor number to 7600 dramatically changes the pressure distribution at this Reynolds number. First, large radial pressure gradients are present due to the centrifugal forces acting on the fluid. Also, for $x/L < 0.5$, the leakage flow pressure decreases in the streamwise direction due to flow

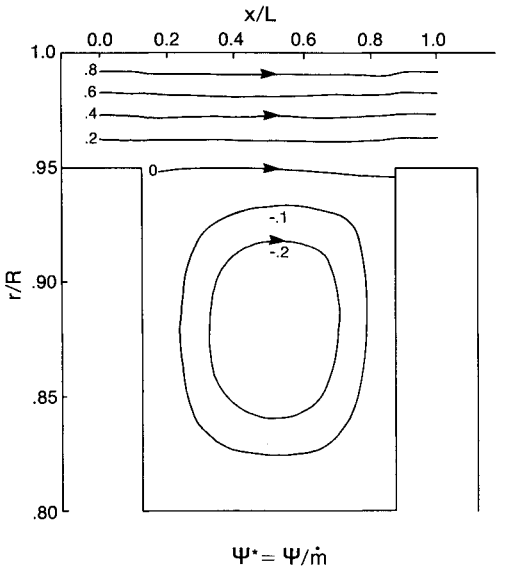

a) $Re = 17{,}880$, $Ta = 0$

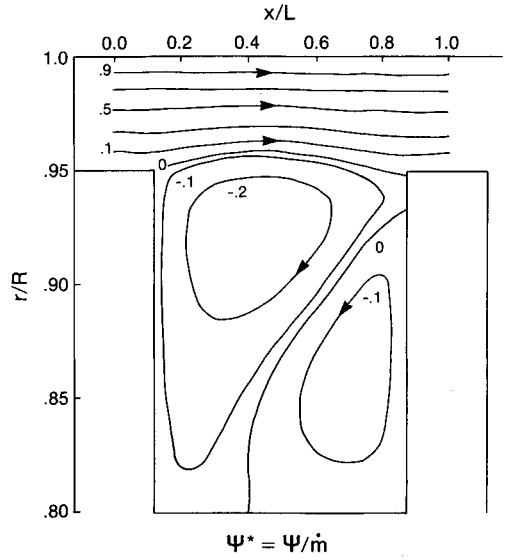

b) $Re = 17{,}340$, $Ta = 19{,}000$

Fig. 5 Predicted streamline pattern.

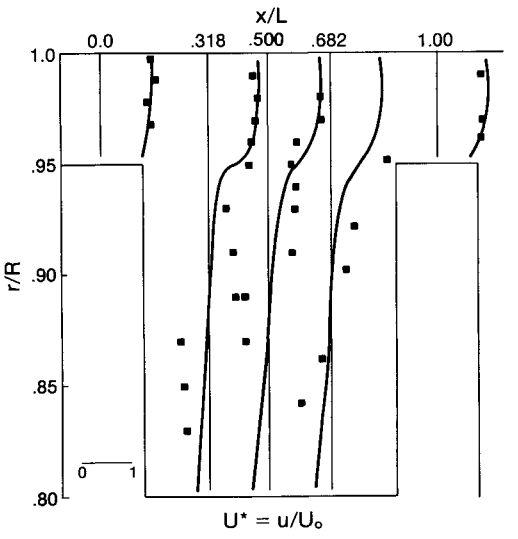

a) $Re = 17{,}880$, $Ta = 0$

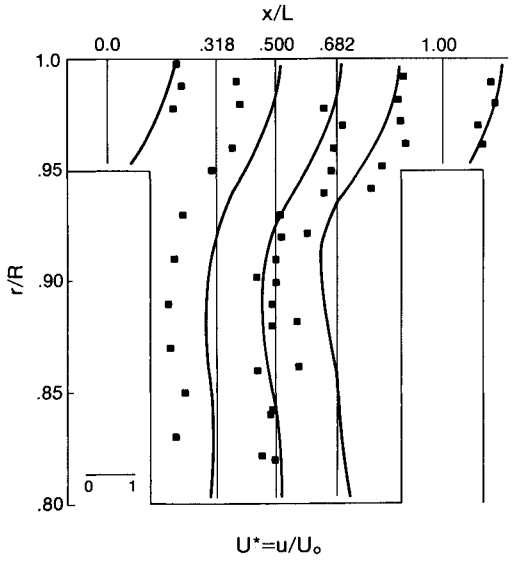

b) $Re = 17{,}340$, $Ta = 19{,}000$

Fig. 6 Predicted (——) and measured (□ □ □) mean axial velocity.

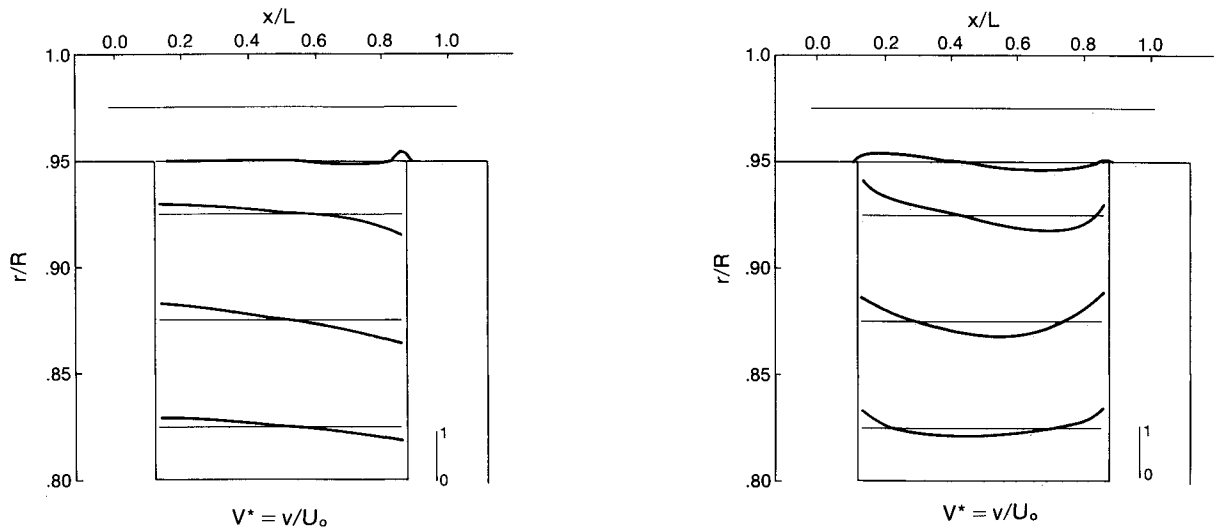

a) $Re = 17{,}880$, $Ta = 0$ b) $Re = 17{,}340$ $Ta = 19{,}000$

Fig. 7 Predicted mean radial velocity.

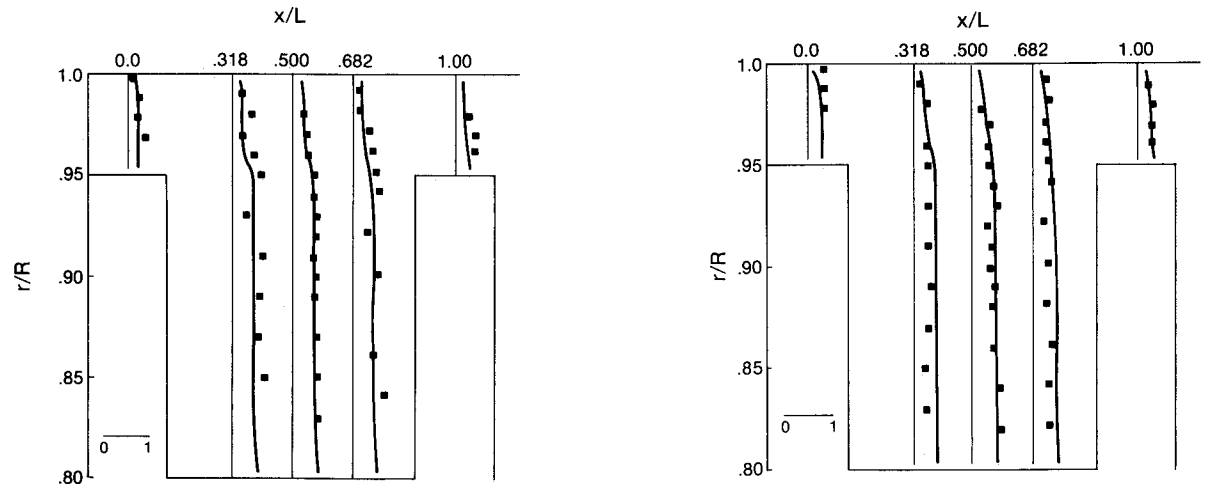

a) $Re = 16{,}920$, $Ta = 7{,}600$ b) $Re = 17{,}340$, $Ta = 19{,}000$

Fig. 8 Predicted (——) and measured (□ □ □) mean swirl velocity

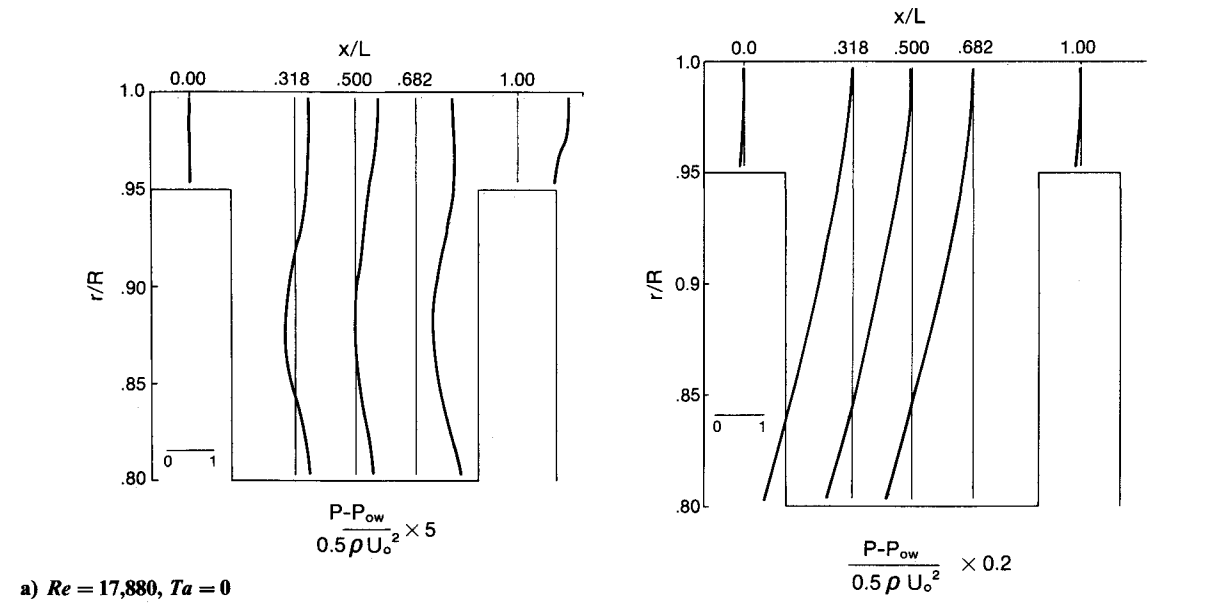

a) $Re = 17{,}880$, $Ta = 0$ b) $Re = 17{,}340$, $Ta = 19{,}000$

Fig. 9 Predicted relative pressure.

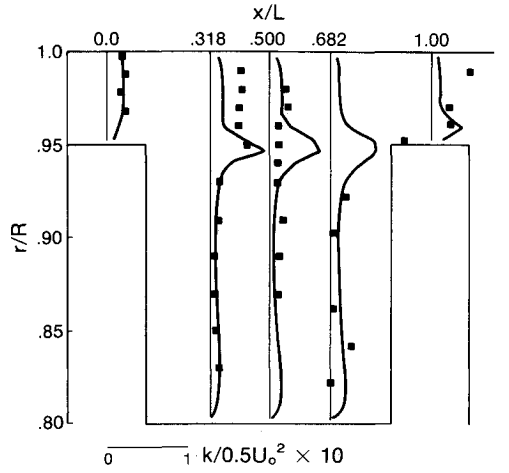

a) $Re = 17{,}880$, $Ta = 0$

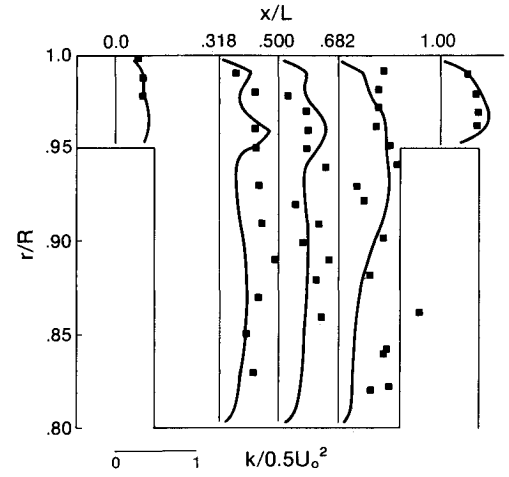

b) $Re = 17{,}340$, $Ta = 19{,}000$

Fig. 10 Predicted (——) and measured (□ □ □) turbulent kinetic energy.

acceleration caused by the outward curved dividing streamline and turbulence dissipation. For $x/L > 0.5$, the flow velocity decreases, and in turn, the pressure increases due to the Bernoulli effect. Finally, for $Ta = 19{,}000$ the radial pressure gradients have dramatically increased. The same characteristic pressure drop is present. One difference over the lower Taylor number case is that the pressure at the exit plane is lower than the inlet pressure. The SRZ produces this added pressure drop by increasing turbulence dissipation of pressure in the flowfield.

By observing the turbulence kinetic energy levels for the nonswirl and strong swirl cases in Figs. 10a and 10b, some idea of the dissipation level may be obtained. For $Ta = 0$, dimensionless turbulence kinetic energy is about 0.06 in the shear layer. Inside the cavity, this value drops to less than 0.01 at the center. For this condition, the turbulence level and, hence, dissipation is extremely low. At $Ta = 7600$ (not shown) and 19,000, the levels are 0.144 and 0.60 in the shear layer and 0.028 and 0.36 in the center of the cavity. Without swirl, there is little turbulence generated except in a very localized region in the shear layer. The development of the second vortex (SRZ) contributes further to the generation of turbulence and the dissipation of the flow energy as a consequence.

V. Conclusions

Two flow regimes are shown to occur in a labyrinth seal. The first is characterized by a single vortex in the cavity region and exists at low Taylor numbers. The second flow regime is characterized by two counter-rotating vortices in the cavity that result in a dramatic increase in the pressure drop across the cavity. From a seal designers standpoint, the presence of the second recirculation zone (SRZ) is desirable, since for a given pressure drop across a seal the leakage rate is lower than if the SRZ was not present.

The SRZ is produced when centrifugal forces become important compared to other forces affecting the flowfield. The growth of the SRZ starts in the lower right-hand corner of the labyrinth cavity and proceeds to divide the cavity diagonally in half as the Taylor number is increased at constant *Re*. A flow regime map is presented showing the conditions at which the SRZ begins to form. It was demonstrated that the required Taylor number necessary to produce this phenomenon could only be achieved at prohibitively large shaft speeds.

The pressure drop across a labyrinth cavity for a given leakage rate is expressed as a loss coefficient C_L. The substantial dependence of this loss coefficient on the Taylor number and the Reynolds number is also shown. A dramatic increase in C_L occurs in the presence of the SRZ.

Acknowledgment

The financial support of the Air Force Office of Scientific Research and NASA Marshall Space Flight Center are gratefully acknowledged.

References

[1]Ludwig, L. P. and Bill, R. C., "Gas Path Sealing in Turbine Engines," NASA TM-73890, 1978.

[2]Stoff, H., "Incompressible Flow in a Labyrinth Seal," *Journal of Fluid Mechanics*, Vol. 100, 1980, pp. 817–829.

[3]Rhode, D. L., Demko, J. A., Traegner, U. K., Morrison, G. L., and Sobolik, S. R., "The Prediction of Incompressible Flow in Labyrinth Seals," *ASME Journal of Fluids Engineering*, Vol. 108, March 1986, pp. 19–25.

[4]Rhode, D. L., Ko, S. H., and Morrison, G. L., "Design Optimization and Testing of a Pump Wear Ring Labyrinth Seal," AIAA Paper 88-3694, July 1988.

[5]Rhode, D. L., Ko, S. H., and Morrison, G. L., "Numerical and Experimental Evaluation of a New Low-Leakage Labyrinth Seal," AIAA Paper 88-2884, July 1988.

[6]Launder, B. E. and Spalding, D. B., "The Numerical Computation of Turbulent Flows," *Computer Methods in Applied Mechanics and Engineering*, Vol. 3, 1974, pp. 269–289.

[7]Lumley, J. L., "Turbulence Modelling," *Journal of Applied Mechanics*, Vol. 50, Dec. 1983, pp. 1097–1103.

[8]Abujelala, M. T. and Lilley, D. G., "Limitations and Empirical Extensions of the k-ε Model as Applied to Turbulent Confined Swirling Flows," AIAA Paper 84-0441, Jan. 1984.

[9]De Vahl Davis, G. and Mallinson, G. D., "False Diffusion in Numerical Fluid Mechanics," Univ. of New South Wales Rept. 1972/FMT/1, May 1972.

[10]Leonard, B. P., "A Stable and Accurate Convective Modelling Procedure Based on Quadratic Upstream Interpolation," *Computer Methods in Applied Mechanics and Engineering*, Vol. 19, June 1979, pp. 59–98.

[11]Leschziner, M. A. and Rodi, W., "Calculations of Various Annular and Twin Jets Using Various Discretization Schemes and Turbulence Model Variations," *ASME Journal of Fluids Engineering*, Vol. 103, June 1981, pp. 352–360.

[12]Leschziner, M. A., "Practical Evaluation of Three Finite Difference Schemes for the Computation of Steady-State Recirculating Flows," *Computer Methods in Applied Mechanics and Engineering*, Vol. 23, Sept. 1980, pp. 293–312.

[13]Han, T., Humphrey, J. A. C., and Launder, B. E., "A Comparison of Hybrid and Quadratic-Upstream Differencing in High Reynolds Number Elliptic Flows," *Computer Methods in Applied Mechanics and Engineering*, Vol. 29, 1981, pp. 81–95.

[14]Launder, B. E. and Spalding, D. B., *Mathematical Models of Turbulence*, Academic Press, London, England, 1972.

[15]Patankar, S. V., *Numerical Heat Transfer and Fluid Flow*, Hemisphere, New York, 1980.

[16]Demko, J. A., "The Prediction and Measurement of Incompressible Flow in a Labyrinth Seal," Ph.D. Dissertation, Texas A&M Univ., College Station, TX, May 1986.

[17]Morrison, G. L., Rhode, D. L., Cogan, K. C., Chi, D., and Demko, J. A., "Labyrinth Seals for Incompressible Flow," Final Report for NASA Contract NAS8-34536, Nov. 1983.